Chapter 3
Flow in Porous Media

3.1 Introduction

As mentioned in Chap. 1, a porous medium is a particulate phase (usually solid) that contains void spaces (microscopic pores). These pores may either be connected to each other or unconnected, and are distributed in the medium in either a regular or a random manner. Porous media can be distinguished as *granular* or *fractured* in form with either *consolidated* or *unconsolidated* mechanical properties. In a consolidated porous medium, the particles (grains) are connected by an intermediate cementing material, while in an unconsolidated porous medium the grains are loose.

The spatial distribution of matter in a porous medium can be typically represented by the phase function $Z(\mathbf{x})$, defined as:

$$Z(\mathbf{x}) = \begin{cases} 1 & \mathbf{x} \text{ belongs to the pore space} \\ 0 & \text{otherwise} \end{cases} \tag{3.1}$$

where $\mathbf{x}$ is the position vector from an arbitrary origin.

The motion of a continuum is generally described by a usually linear relation between some fluxes and the relative driving forces. Following the trend of *determinism*, a large number of constitutive (phenomenological) equations describing relationships between fluxes and driving forces exist in several fields of physics. These include Newton's law (which correlates developing forces with acceleration, i.e. velocity gradient), Fourier's law (which correlates heat flow with temperature gradient), Fick's law (which correlates mass flow with concentration gradient), Ohm's law (which correlates current with potential gradient), etc. The description of flow in porous media is especially difficult due to the media's complex geometry. Furthermore, a general law of the continuum theory is the law of conservation of extensive properties such as mass, momentum and energy. The resulting equations of continuity are commonly referred to as field equations and must be considered along with flow equations to adequately describe flow in porous structures.

F. A. Coutelieris and J. M. P. Q. Delgado, *Transport Processes in Porous Media*, Advanced Structured Materials 20, DOI: 10.1007/978-3-642-27910-2_3,

Experimental and theoretical investigations are normally associated with the scale of the application considered. In general, these scales are microscopic (or "pore" scale), mesoscopic (or "local" scale), and macroscopic (or "field" scale). As far as the phenomena considered (and the governing equations as well as the relative solutions) are strongly dependent on the scale, the transition between different scales is of great importance. This transition is usually considered from the lowest "pore" level, where experimental and simulation results could be easily obtained, to the higher "field" scale, where data are hard to be measured. This up-scaling process is the subject of many studies (see Sects. 5.5 and 7.5).

3.1.1 Macroscopic Description

During his experiments on flow in pipes, Darcy found and proved that the pressure drop caused by the flow is proportional to the velocity. This result is expressed by the phenomenological Darcy law equation [7]:

$$q = A\frac{k}{\mu}\frac{\Delta p}{L} \tag{3.2}$$

which generally describes the fluid flow through a porous medium. In the above formula, q is the volumetric flowrate through a cross-section, A of the porous medium, which is perpendicular to the flow direction, L is the length of the porous media in direction of flow, Δp is the pressure difference along the porous medium, μ is the viscosity of the flowing fluid, and k is the permeability as a material property of the porous medium. This equation can be written in differential form as:

$$\nabla p = -\frac{\mu}{k}\mathbf{u} \tag{3.3}$$

where $\mathbf{u}$ denotes the velocity vector of the fluid. It is important to note that the Darcy law is only valid for a laminar and steady state one-phase flow through a porous medium. In addition, the fluid must be largely incompressible.

An extension to the Darcy law is the isotropic law introduced by Brinkman law [3]:

$$\nabla p = -\frac{\mu}{k}\mathbf{u} + \mu_{eff}\nabla^2\mathbf{u} \tag{3.4}$$

where μ_{eff} is an effective viscosity which may be different from μ. The Brinkman law is a slight modification of the Stokes equation and one of its practical advantages is that applications and analytical tools devoted to the Stokes approach can be used with small adaptations.

One of the most significant applications of Darcy's law (3.2) is the calculation of permeability of a porous material. After solving the equation for k:

$$k = \frac{q}{A}\mu\frac{L}{\Delta p} \tag{3.5}$$

the permeability of a porous media is defined as 1 Darcy, if a fluid of 1 cP viscosity, flowing through a cross-section of 1 cm^2 at a rate of 1 cm^3/s, causes a pressure drop of 1 atm/cm. Many years later, Klinkenberg observed that gas permeability is not the same as liquid permeability for the same porous structure, since gas permeability depends on pressure [16]. The correlation between gas permeability k_{gas}, liquid permeability k_{liq} and mean pressure inside the core p_{mean}, is given as:

$$k_{gas} = k_{liq}\left(1 + \frac{b}{p_{mean}}\right) \tag{3.6}$$

where parameter b depends on the gas studied.

All the above calculations are valid under the major restriction that permeability should be a number, which means that the porous medium is homogeneous and isotropic. For non-homogeneous and anisotropic media, permeability becomes a *tensor*, thus the above equations should be transformed accordingly.

3.1.2 Microscopic Description

Modeling approaches for microscopic conditions can be described by the appropriate flow conditions equations (creeping, laminar, turbulent, etc.). It is important to note that these equations are defined in the pore space, therefore the boundary conditions in the solid–fluid interface are essential to solve the flow problem. Obviously, equations of motion and the accompanying boundary conditions, are strongly dependent on the application considered, thus many different approaches have been proposed in the literature. The problem here is the derivation of representative macroscopic quantities *from* the microscopic results, a procedure which hardly allows for a generalized unique solution. As the extensive discussion of these issues is not within the scope of this book, our presentation is limited to *granular porous media*, where analytical solutions are also available through the cell models.

3.2 Analytical Solutions for Single Phase Flow in Cell Models

As mentioned in Chap. 2, cell models have been widely used for mathematical simulation of the flow conditions through porous structures, especially granular materials. According to these models, the grains are distributed throughout the predefined space, and each grain is enclosed in a cell formed by the liquid phase. The cell model can be used to reduce the solution of the boundary-value problem for the flow around a system of particles to the problem for a single particle, where the flow field solution can be obtained by the analytical solution of the Stokes problem. The cell models differ in their boundary conditions, as discussed below. A wide variety of assumptions exists for the shape of the grains, and the cells in general: spherical, cylindrical, spheroidal, etc. Different approaches for the physical

conditions and mathematical formulations have also been presented for each geometry considered, therefore producing an extensive range of combinations between geometrical and physical considerations. These combinations are described below.

3.2.1 Sphere-in-Cell Models: Kuwabara's Approach

Consider a solid sphere of radius α, surrounded by another concentric spherical liquid envelope of radius β, whose thickness is adjusted so the porosity of the medium is equal to that of the model. The internal sphere is solid and stationary while a Newtonian fluid flows around the solid core under constant approaching velocity. The governing equation for quasi-steady creeping flow of incompressible (i.e. constant density) viscous (i.e. constant dynamic viscosity) fluids is the well-known Stokes equation, given as:

$$\nabla p = \mu \nabla^2 \mathbf{v} \tag{3.7}$$

along with the continuity equation:

$$\nabla \cdot \mathbf{v} = 0 \tag{3.8}$$

where p is the pressure field, $\mathbf{v}$ is the velocity vector, and μ is the dynamic viscosity. As the system is axially symmetrical, the problem is two-dimensional. Accordingly, by using the spherical coordinates system (r, θ), the above equation can be written in terms of the steam-function ψ, as:

$$\mathrm{E}^2\left(\mathrm{E}^2 \psi\right) = 0 \tag{3.9}$$

where:

$$\mathrm{E}^2 = \frac{\vartheta^2}{\vartheta r^2} - \frac{\sin\theta}{r^2}\frac{\vartheta^2}{\vartheta \theta^2} \tag{3.10}$$

Consequently, the velocity components are given as:

$$u_r = -\frac{1}{r^2 \sin\theta}\frac{\vartheta \psi}{\vartheta \theta}, \quad u_\theta = \frac{1}{r \sin\theta}\frac{\vartheta \psi}{\vartheta r} \tag{3.11}$$

To solve the above problem, it is necessary to consider the appropriate boundary conditions. According to Kuwabara's approach [17], zero vorticity is assumed on the outer surface, as depicted in Fig. 3.1.

The velocity components are expressed as:

$$u_r = -2\left[\frac{F_1}{r^3} + \frac{F_2}{r} + F_3 + F_4 r^2\right]\cos\theta \tag{3.12}$$

$$u_\theta = -\left[\frac{F_1}{r^3} - \frac{F_2}{r} - 2F_3 - 4F_4 r^2\right]\sin\theta \tag{3.13}$$

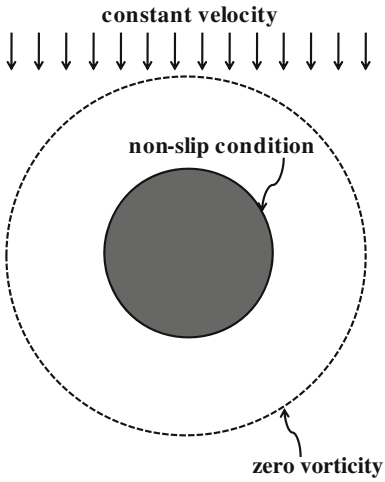

Fig. 3.1 Kuwabara's sphere-in-cell model

where:

$$F_1 = -\frac{U_\infty}{4F_5}\left(1 - 2\frac{\alpha^3}{\beta^3}\right) \tag{3.14}$$

$$F_2 = -\frac{3U_\infty}{4F_5} \tag{3.15}$$

$$F_3 = -\frac{U_\infty}{2F_5}\left(1 + \frac{\alpha^3}{2\beta^3}\right) \tag{3.16}$$

$$F_4 = -\frac{3U_\infty}{20F_5}\left(\frac{\beta^3}{\alpha^3}\right) \tag{3.17}$$

$$F_5 = \left(1 - \frac{\alpha}{\beta}\right)^3 \left(1 + \frac{6\beta}{5\alpha} + \frac{3\beta^2}{5\alpha^2} + \frac{\beta^3}{5\alpha^3}\right) \tag{3.18}$$

and where U_∞ is the magnitude of the uniform approaching velocity.

Typical results for the stream function are presented in Fig. 3.2 which also depicts a comparison with Happel's approach (for details on Happel's model, see Sect. 3.2.2).

3.2.2 Sphere-in-Cell Models: Happel's Approach

The model proposed by Happel [10, 11] is similar to that of Kuwabara but differs in the fluid motion. Kuwabara's stationary grain is located in a flowing fluid, however, Happel proposed a grain moving under constant velocity in an otherwise

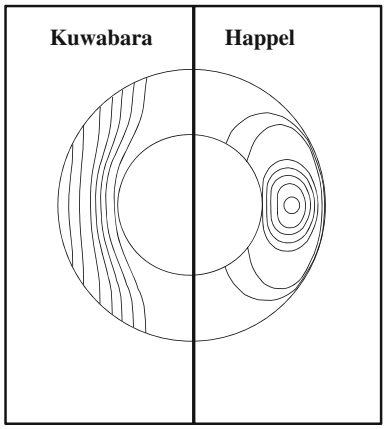

Fig. 3.2 Sample stream lines in two sphere-in-cell models

quiescent surrounding fluid. This dissimilarity imposes different boundary conditions, as depicted in Fig. 3.3.

Compared to Kuwabara's approach, Happel's model has the additional advantage of being autonomous from an energy point of view. This benefit is the main reason for the wider acceptance of Happel's approach rather than Kuwabara's model.

In Happel's approach, the governing equations are the same as (3.7–3.11), where it is assumed that the solid spherical core is moving under a constant velocity gradient q. After all, the velocity components are expressed as [10]:

$$u_r = \left[6r^3F_1 + 2rF_2 + \frac{6}{r^2}F_3 - \frac{3}{r^4}F_4 + rq\right]\sin\theta\cos\theta \tag{3.19}$$

$$u_\theta = \left[5r^3F_1 + rF_2 + \frac{1}{r^4}F_4 + \frac{rq}{2}\right]\left(\cos^2\theta - \sin^2\theta\right) \tag{3.20}$$

where:

$$F_1 = -\frac{5q}{4\alpha^2}\left(\frac{\left(\frac{\alpha}{\beta}\right)^7}{10 + 4\left(\frac{\alpha}{\beta}\right)^7}\right)F_5 \tag{3.21}$$

$$F_2 = \frac{5q}{4}\left(\frac{4 + 10\left(\frac{\alpha}{\beta}\right)^7}{10 + 4\left(\frac{\alpha}{\beta}\right)^7}\right)F_5 - \frac{q}{2} \tag{3.22}$$

$$F_3 = -\frac{5q\alpha^3}{12}F_5 \tag{3.23}$$

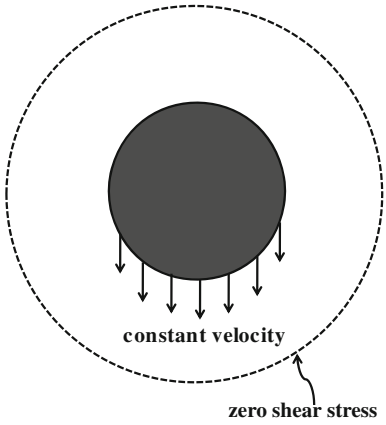

Fig. 3.3 Happel's sphere-in-cell model

$$F_4 = -\frac{5\alpha^5}{10 + 4\left(\frac{\alpha}{\beta}\right)^7} F_5 \tag{3.24}$$

$$F_5 = \frac{10 + 4\left(\frac{\alpha}{\beta}\right)^7}{10\left[1 - \left(\frac{\alpha}{\beta}\right)^{10}\right] - 25\left(\frac{\alpha}{\beta}\right)^3\left[1 - \left(\frac{\alpha}{\beta}\right)^4\right]} \tag{3.25}$$

The visual interpretation of sample flow in Happel's sphere-in-cell is depicted in Fig. 3.2.

3.2.3 Cylinder-in-Cell Models

Further to "sphere-in-cell" models, both Happel and Kuwabara also proposed similar "cylinder-in-cell" ones. The similarity in the formulations and the consequent analytical solutions is due to the two-dimensionality of the mathematical description that allows us to ignore the shape imposed by the third dimension.

3.2.4 Spheroid-in-Cell Model

As described above, grain are often closer in shape to spheroids rather than spheres. This observation leads to the development of "spheroidal-in-cell" models, similar to those of Happel and Kuwabara. One difficulty of such a mathematical interpretation arises from the orientation of the spheroidal geometry, which can be either *prolate* or *oblate*, as illustrated in Fig. 3.4.

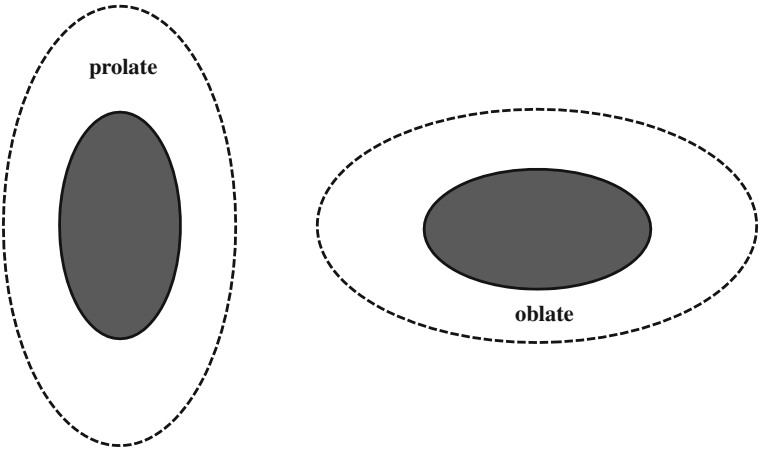

Fig. 3.4 Prolate and oblate spheroidal cells

In cases of prolate geometry, the inner solid spheroid has long semiaxis a_3 and short semiaxis a_1, where $a_3 > a_1$. The semifocal distance a is defined as $a = \sqrt{a_3^2 - a_1^2}$. The outer confocal prolate spheroid is of long and short semiaxes b_3 and b_1, respectively, while its dimensions are determined so that the volume fraction of the spheroid-in-cell is equal to that of the original swarm of spheroidal particles. Thus, given the dimensions of the inner spheroid, porosity is related to the outer semiaxes by the following equations:

$$(1 - \varepsilon) b_1^2 b_3 = a_3 \tag{3.26}$$

$$b_1 = \sqrt{b_3^2 - a^2} \tag{3.27}$$

The axisymmetric, steady state, incompressible, viscous creeping flow is again described in terms of stream function by Eq. 3.9, where the operator E^2 is given as:

$$E^2 = \frac{1}{\alpha^2 \left(\sinh^2 \eta + \sin^2 \theta \right)} \left[\coth^2 \eta \frac{\partial^2}{\partial \eta^2} - \coth^2 \eta \frac{\partial}{\partial \eta} + \frac{\partial^2}{\partial \theta^2} - \cot \theta \frac{\partial}{\partial \theta} \right] \tag{3.28}$$

Under this respect, the velocity components are given in the prolate spheroidal coordinates system (η, θ) as [20]:

$$u_\eta = \frac{-1}{\alpha^2 \sqrt{\sinh^2 \eta + \sin^2 \theta} \sinh \eta \sin \theta} \frac{\partial \psi}{\partial \theta} \tag{3.29}$$

$$u_\theta = \frac{1}{\alpha^2 \sqrt{\sinh^2 \eta + \sin^2 \theta} \sinh \eta \sin \theta} \frac{\partial \psi}{\partial \eta} \tag{3.30}$$

By using the *semi-separation concept* introduced by Dassios et al. [8], the stream function is analytically given by an infinite series expansion of the form:

$$\psi(\eta,\theta)=\sum_{n=2,4,\ldots}^{\infty} g_n(\cosh\eta)G_n(\cos\theta) \tag{3.31}$$

The leading term of the above infinite series has proved to be sufficient enough to adequately represent the whole stream function [4], thus the stream function is given as:

$$\begin{aligned}\psi(\eta,\theta)=\{&A_1G_1(\cosh\eta)+A_2G_2(\cosh\eta)+A_3G_4(\cosh\eta)\\&+A_4H_2(\cosh\eta)\}G_2(\cos\theta)\end{aligned} \tag{3.32}$$

where A_1, A_2, A_3 and A_4 are constants coefficients, the values of which depend on the geometrical parameters η_a and η_β (the values of the coordinate η on the inner and outer surface, respectively). Obviously, their expressions are also dependent on the model considered (Kuwabara or Happel), i.e. on the boundary conditions applied.

More specifically, Kuwabara's approach corresponds to the expression:

$$\begin{aligned}\psi(\eta,\theta)=\frac{\alpha}{D}\Bigg\{&\Lambda_2G_2(\cosh\eta)+\Lambda_3\left[\frac{5G_4(\cosh\eta_\beta)}{G_1(\cosh\eta_\beta)}G_1(\cosh\eta)+G_4(\cosh\eta)\right]\\&+\Lambda_4H_2(\cosh\eta)\Bigg\}G_2(\cos\theta)\end{aligned} \tag{3.33}$$

where D, Λ_2, Λ_3 and Λ_4 are $\eta-$ and $\theta-$ dependent coefficients, defined by Dassios et al. [9], and $G_N(x)$ and $H_N(x)$ are the Gegenbauer polynomials of the first and second kind, respectively, of degree $-\frac{1}{2}$ and order N.

The Happel approach results in the algebraic linear system [9]:

$$\begin{bmatrix} G_1(\cosh\eta_a) & G_2(\cosh\eta_a) & G_4(\cosh\eta_a) & H_2(\cosh\eta_a)\\ G_1'(\cosh\eta_a) & G_2'(\cosh\eta_a) & G_4'(\cosh\eta_a) & H_2'(\cosh\eta_a)\\ G_1(\cosh\eta_\beta) & G_2(\cosh\eta_\beta) & G_4(\cosh\eta_\beta) & H_2(\cosh\eta_\beta)\\ \mathrm{K}G_1''(\cosh\eta_\beta) & \mathrm{K}G_2''(\cosh\eta_\beta) & \mathrm{K}G_4''(\cosh\eta_\beta) & \mathrm{K}H_2''(\cosh\eta_\beta)\\ +\Lambda G_1'(\cosh\eta_\beta) & +\Lambda G_2'(\cosh\eta_\beta) & +\Lambda G_4'(\cosh\eta_\beta) & +\Lambda H_2'(\cosh\eta_\beta) \end{bmatrix}\cdot \begin{bmatrix} A_1\\A_2\\A_3\\A_4 \end{bmatrix}=\begin{bmatrix} MG_2(\cosh\eta_a)\\ MG_1(\cosh\eta_a)\\0\\0 \end{bmatrix} \tag{3.34}$$

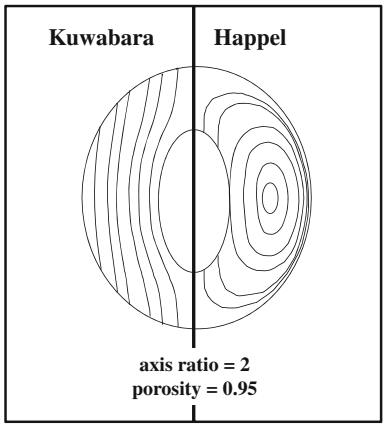

Fig. 3.5 Sample stream lines in two identical prolate spheroids-in-cell

where:

$$\mathrm{K} = \cosh^2 \eta_\beta - \frac{1}{5} \tag{3.35}$$

$$\Lambda = -2 \cosh \eta_\beta \tag{3.36}$$

$$\mathrm{M} = \frac{2}{\cosh^2 \eta_a - 1} \tag{3.37}$$

and where the primes and double primes denote the first and second derivatives of the corresponding functions, respectively.

Some typical results for the flow field in a spheroidal-in-cell are shown in Fig. 3.5.

The spheroid is oblate when $a_3 < a_1$, where the semifocal distance is given by $\bar{a} = \sqrt{a_1^2 - a_3^2}$. As shown by various researchers (see, for example, Happel and Brenner [12]) the stream function for the oblate case can be obtained from the same formulation as above, by using the following transformation from the prolate coordinates system (η, θ) to the oblate one $(\bar{\eta}, \theta)$:

$$\cosh \eta = i \cosh \bar{\eta} \tag{3.38}$$

$$a = -i\bar{a} \tag{3.39}$$

Following this, the solution for stream function can be easily obtained; some typical results of which are shown in Fig. 3.6.

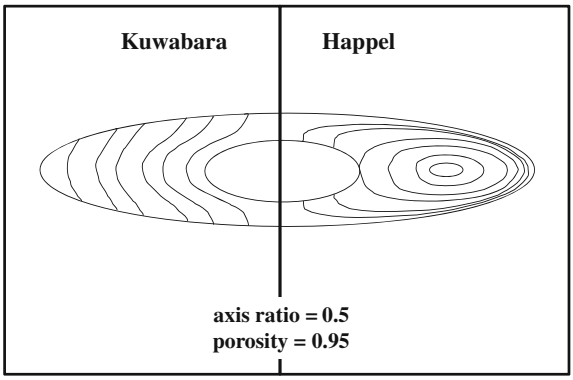

Fig. 3.6 Sample stream lines in two identical oblate spheroids-in-cell

3.3 Single Phase Flow in Granular Structures

In the presence of porous media, the need for a realistic description of the structure of a porous medium significantly increases the mathematical complexity of a model. As porous media are generally characterized by highly complex internal geometry, appropriate modeling is necessary for the derivation of meaningful conclusions. Numerous industrial and technological applications involving fluid flow and mass transport processes within multi-particle assemblages have attracted scientific interest in the last decades, mainly focusing on industrial physicochemical processes (sedimentation, catalysis, etc.), alternative energy sources (fuel cells, etc.), and separation techniques (chromatography, filters, etc.). Although arrays of regularly spatially distributed spheres represent an idealization of real granular media, they have been widely studied from both the fluid dynamics and mass transport points of view [19, 21]. On the other hand, due to their complex geometry, random particle distributions were the subject of rather limited investigations until the 1990s (see [2, 18]). Since then, fast advances in computational capabilities have contributed to reviving interest on this topic with emphasis placed on hydrodynamic aspects [5, 13, 22].

3.3.1 Representation of 3-D Sphere Assemblages

To define a realistic domain to solve flow and transport problems, a granular porous medium was constructed in the form of a spherical particle assemblage. The structure was digitized and the phase function (equal to zero for solid and unity for the pore space) was determined to obtain the specified porosity. More specifically, representation of the domains under consideration was achieved as follows:

Step (1) Using a random number generator, the position of the sphere's center was selected, being in a box of specified dimensions ($3 \times 2 \times 3$ mm)

Step (2) Using a random number generator, a radius assumed to follow the log-normal distribution was selected

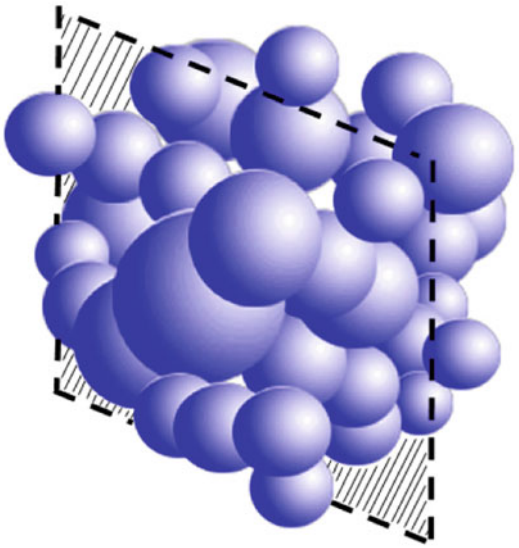

Fig. 3.7 A three-dimensional representation of a porous medium

Step (3) The void space around the sphere was checked. If it was free the radius value was accepted, otherwise Step 2 was repeated
Step (4) The sphere was posed
Step (5) Steps 1–4 were repeated until the volume of the positioned spheres satisfied the pre-defined porosity value.

Obviously, many three-dimensional representations can be generated by the above algorithm for a specific porosity value. Therefore, it is necessary to validate the results against these configurations to ensure that the macroscopic results are independent of each specific realization. A graphic representation of a representative medium for a typical porosity of $\varepsilon = 0.43$ is presented in Fig. 3.7.

A randomly selected two-dimensional cut of this domain in is shown in Fig. 3.8, which also depicts the grid of the numerical solution.

3.3.2 The Flow Field

For the numerical simulations, the velocity field was computed numerically by solving the Stokes equations

$$\nabla p = \mu \nabla^2 \mathbf{v} \tag{3.40}$$

$$\nabla \cdot \mathbf{v} = 0 \tag{3.41}$$

$$\mathbf{v} = 0 \,\text{at liquid} - \text{solid interface} \tag{3.42}$$

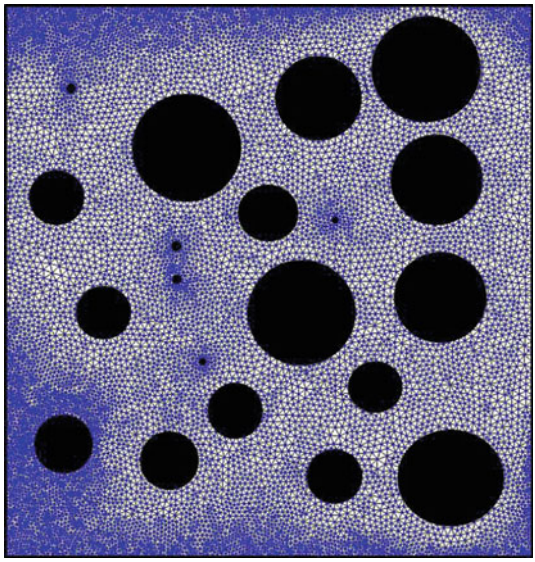

Fig. 3.8 A selected two-dimensional cut of the simulated geometry discretized by an unstructured grid

where $\mathbf{v}$, p, and μ are the velocity vector, pressure field, and fluid viscosity, respectively.

The procedure for solving the Stokes flow problem involves discretization in terms of cubic elements as follows [1, 6, 14, 15]: At the pore level, a staggered marker-and-cell (MAC) mesh is used, with the pressure defined at the center of the cell, and the velocity components defined along the corresponding face boundaries. The resulting linear system of equations is solved by a successive over-relaxation (SOR) method. An initial estimate of p is determined by solving the Laplace equation. Next, the velocity vector $\mathbf{v}$ is calculated from the corresponding momentum balance and the continuity equation $\nabla \cdot \mathbf{v} = 0$. The pressure is corrected through an artificial compressibility equation of the form:

$$\frac{dp}{dt} = \nabla \cdot \mathbf{v} \tag{3.43}$$

Essentially, the method adds an artificial density time derivative related to the pressure by an artificial equation of state $p = \beta\rho$, where β is an artificial compressibility factor. Similar to the compressible momentum equation, $c = \beta^{1/2}$ is an artificial speed of sound and for stability during the iterative procedure, its magnitude should be such that the respective artificial Mach number, $M = \frac{R}{c}\max_D\left(\sum_i u_i^2\right)^{1/2}$ is low (M $\ll$ 1), where R is the relevant Reynolds number. In the limiting case of R $\to$ 0, which is the present case, any finite value of β should meet this criterion. Thus, $\beta = 1$ was selected although it is evident that the

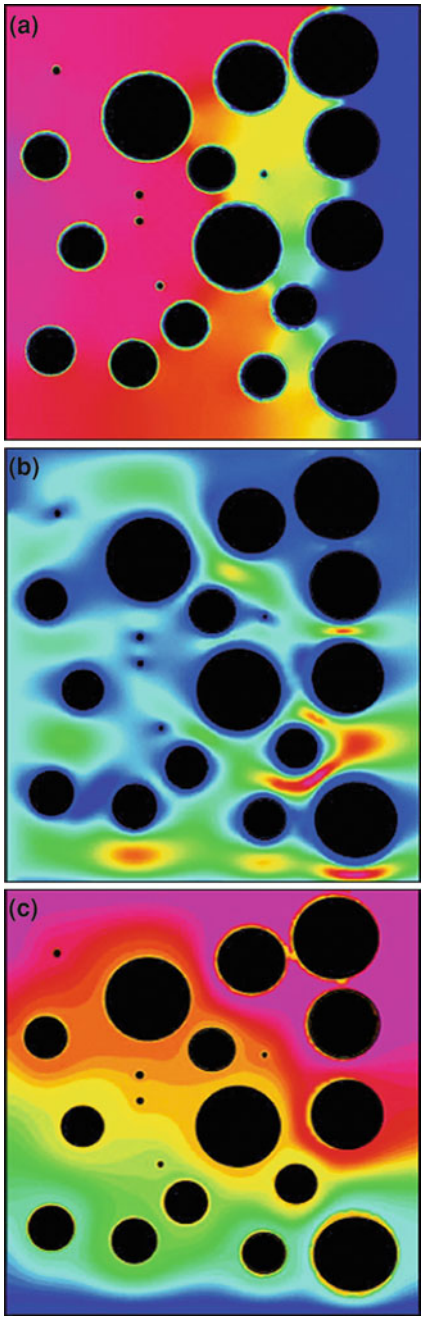

Fig. 3.9 Snapshot of the **a** pressure field, **b** velocity, and **c** stream line simulations through the representative porous medium. The flow direction is from *left* to *right*

exact value cannot have any effect on the final (steady state) results, since at steady state the artificial density time derivative is equal to zero.

The above steps are repeated until convergence is reached. This numerical scheme for the determination of the velocity field has been widely validated in terms of both the velocity field and the corresponding permeability [1, 6, 14, 15].

3.3.3 Results and Discussion

Figure 3.9 show the results of the (a) pressure field, (b) velocity, and (c) stream function for a typical porous medium of $\varepsilon = 0.72$. A randomly selected two-dimensional cut of the medium is considered so the results can be visualized clearly. The boundary condition at the closed walls is non-slip, at the left boundary an inflow was imposed, and at the right boundary an outflow condition. Small vortices and recirculating flow are produced in the medium depending on the pore size, while smoother profiles are obtained at the inlet and outlet. The velocity gradient observed from top to bottom at the inlet surface is generated because the inflow condition ensures constant molar flux instead of a plug-type velocity vector. Finally, it is interesting to observe that the faster flow paths are generated by the porous structure and they appear wherever pore diameters are fairly small.

References

1. Adler, P.M., Jacquin, C.J., Quiblier, J.A.: Flow in simulated porous media. Int J Multiphas Flow **16**, 691–712 (1990)
2. Berryman, J.G.: Effective conductivity by fluid analogy for a porous insulator filled with a conductor. Phys. Rev. B **27**, 7789–7792 (1983)
3. Brinkman, H.C.: A calculation of the viscous force exerted by a flowing fluid on a dense swarm of particles. Appl. Sci. Res. A **1**, 27–34 (1949)
4. Burganos, V.N., Coutelieris, F.A., Dassios, G., Payatakes, A.C.: On the rapid convergence of the analytical solution of stokes flow around spheroids-in-cells. Chem. Eng. Sci. **50**, 3313–3317 (1995)
5. Coelho, D., Thovert, J.F., Adler, P.M.: Geometrical and transport properties of random packings of spheres and aspherical particles. Phys. Rev. E **55**, 1959–1978 (1997)
6. Coutelieris, F.A., Kainourgiakis, M.E., Stubos, A.K.: Low peclet mass transport in assemblages of spherical particles for two different adsorption mechanisms. J. Colloid Interface Sci. **264**, 20–29 (2003)
7. Darcy H (1857) Recherches Experimentales Relatives au Mouvement de l'Eau dans les Tuyaux, Mallet-Bachelier, Paris
8. Dassios, G., Hadjinicolaou, M., Payatakes, A.C.: Generalized eigenfunctions and complete semiseparable solutions for stokes flow in spheroidal coordinates. Quart. Appl. Math. **52**, 157–191 (1994)
9. Dassios, G., Hadjinicolaou, M., Coutelieris, F.A., Payatakes, A.C.: Stokes flow in spheroidal particle-in-cell models with Happel and Kuwabara boundary conditions. Int. J. Eng. Sci. **33**, 1465–1490 (1995)

10. Happel, J.: Viscosity of suspensions of uniform spheres. J. Appl. Phys. **28**, 1288–1292 (1957)
11. Happel, J.: Viscous flow in multiparticle systems: Slow motion of fluids relative to beds of spherical particles. AIChE J. **4**, 197–201 (1958)
12. Happel, J., Brenner, H.: Low Reynolds Number Hydrodynamics. Prentice-Hall, Englewood Cliffs (1965)
13. Jullien, R., Meakin, P.: Simple three-dimensional models for ballistic deposition with restructuring. Europhys. Lett. **4**, 1385–1390 (1987)
14. Kainourgiakis, M.E., Kikkinides, E.S., Stubos, A.K.: Diffusion and flow in porous domains constructed using process-based and stochastic techniques. J. Porous. Mat. **9**, 141–154 (2002)
15. Kikkinides, E.S., Burganos, V.N.: Permeation properties of three-dimensional self-affine reconstructions of porous materials. Phys. Rev. E **62**, 6906–6915 (2000)
16. Klinkenberg, L.J.: The permeability of porous media to liquids and gases, drilling and production practice. Am. Petr. Inst. **V**, 200–213 (1941)
17. Kuwabara, S.: The forces experienced by randomly distributed parallel circular cylinder or spheres in a viscous flow at small Reynolds numbers. J. Phys. Soc. Jpn. **14**, 527–532 (1959)
18. Meakin, P., Skjeltorp, A.T.: Application of experimental and numerical models to the physics of multiparticle systems. Adv. Phys. **42**, 1–127 (1993)
19. Meredith, R.E., Tobias, C.W.: Resistance to potential flow through a cubical array of spheres. J. Appl. Phys. **31**, 1270–1273 (1960)
20. Moon, P., Spencer, D.E.: Field Theory Handbook: Including Coordinate Systems, Differential Equations, and Their Solutions, 2nd edn. Springer, Berlin (1971)
21. Rayleigh, R.S.: On the influence of obstacles arranged in rectangular order upon the properties of a medium. Philos. Mag. **34**, 481–502 (1892)
22. Visscher, W.M., Bolsterli, M.: Random packing of equal and unequal spheres in two and three dimensions. Nature **239**, 504–507 (1972)